Adv. Manuf.
https://doi.org/10.1007/s40436-026-00609-9

# Unlocking the potential of friction stir extrusion as a sole manufacturing step for producing sustainable tubes from aluminum chips

**Muhammad Adnan[1] · Riccardo Puleo[1] · Gianluca Buffa[1] · Livan Fratini[1] · Giuseppe Ingarao[1]**

Received: 6 August 2025 / Revised: 30 September 2025 / Accepted: 15 April 2026


**Abstract** Conventional remelting-based methods are widely used for recycling aluminium alloys scraps; however, these approaches come with significant drawbacks, including high energy consumption, permanent material losses, reduced purity, and low mechanical properties. To address these issues, solid state techniques have emerged over the last years as environmentally friendly recycling processes. Among them, friction stir extrusion (FSE) has proved to be a promising technique for producing wires/rods directly from metallic chips. In order to cover the market demand of semifinished product shapes, this study explores the possibility to produce aluminium alloys tube directly from chips without intermediate steps. This would save energy and resources, strengthening the environmental sustainability performance of FSE based recycling processes. An experimental and numerical approach is here proposed and the impacts of the main process parameters on the microstructural and mechanical properties of extruded aluminium tubes are analyzed. Results revealed that FSE could be used as sole process step to produce tubes from chips, and mechanical and microstructural analysis showed a substantial increase in hardness in correspondence to very fine and equiaxed grain structure. Moreover, numerical simulations were used to explain the small variations observed in grain size. Lastly, the electrical energy demand of this single-step approach was compared with that of conventional multi-step routes, demonstrating its superior energy efficiency.

✉ Riccardo Puleo
riccardo.puleo01@unipa.it

[1] Department of Engineering, University of Palermo, 90128 Palermo, Italy

**Keywords** Friction stir extrusion (FSE) · Tubes · Recycling · Extrusion · Mechanical · Microstructure · Solid bonding

## 1 Introduction

Recently, the use of lightweight parts has been increasing with the development of the automotive and aerospace industries. The automobile industry has gradually increased the use of lightweight materials such as aluminium alloys, due to an increase in the restriction of exhaust gas and the improvement of the combustion ratio [1]. As a component in lightweight aerospace and automobile parts, the production of Al tubes with high strength and extrudability, such as those needed for door impact beams, seat side rails, and hood support, is in demand.

Aluminium production is highly energy-intensive, primarily relying on electrolytic reduction processes that consume large amounts of electricity [2]. Energy costs account for 20%–40% of overall production expenses [3]. Consequently, recycling aluminium alloys presents a more sustainable alternative, reducing both energy consumption and environmental impact. Studies suggest that aluminium recycling can mitigate up to 94% of the environmental effects related to global warming and fossil fuel depletion [2].

Conventional aluminium recycling methods, including remelting and recasting, are energy-intensive and lead to significant material losses due to oxidation [4]. To address these challenges, solid-state recycling (SSR) techniques have been developed, which process alloy scraps through plastic deformation below the solidus temperature [5]. This method drastically reduces energy consumption to just 5% of that required by traditional remelting methods and retains up to 95% of the original material, minimizing losses caused by

Published online: 22 May 2026

oxidation, burning, and slag contamination [6]. Within the SSR category, it is worth mentioning equal channel angular pressing (ECAP) [7], shear assisted processing and extrusion (ShAPE) [8], hot extrusion, and hot rolling method [9], consolidation [10], forging [9], and sintering [11].

In the literature, friction-based processes, another family of processes, namely, belong to the SSR processes. An example is the friction stir extrusion (FSE), which is an emerging solid-state recycling technique that takes advantage of the process mechanics of friction stir welding (FSW). It utilizes frictional heat and mechanical deformation to extrude metal, allowing for direct conversion of metal powders, chips, or billets into high-quality products [6]. FSE has gained attention due to its capability to manufacture finished or semi-finished products while providing superior material properties, such as enhanced strength, structural integrity, and corrosion resistance. In fact, FSE effectively addresses challenges associated with conventional recycling, such as alloy segregation and degradation due to high temperatures [12], thus, supporting sustainable manufacturing and circular economy principles in the metallurgical industry.

A few researchers have investigated FSE techniques for recycling lightweight materials. Buffa et al. [13] examined how tool rotation and force influenced mechanical properties and microhardness in thin aluminium wires, highlighting that a tapered shoulder shape improved solid bonding. Baffari et al. [14] explored FSE's role in reforming aluminium chips into metal matrix composites, finding that increased reinforcement powder led to intergranular sedimentation and cracking. Adnan et al. [15] studied the effect of reinforced SiC on the mechanical and microstructural properties of aluminium wire extruded by the FSE process. The authors found that SiC-reinforced composite wire enhanced properties compared to the unreinforced wire. Sharifzadeh et al. [16] assessed the corrosion resistance and wear properties of magnesium rods manufactured through FSE, determining that optimal rotational speeds resulted in superior surface quality and mechanical strength.

Apart from wire and rod production, the FSE process can be effectively implemented for tube production. Milner and Abu-Farha [17] examined FSE in lightweight tube manufacturing, assessing the impact of process parameters on magnesium tubes' microstructure. Their results showed that friction stir extruded samples exhibited a 28% reduction in yield strength compared to the base material. Zhang et al. [18] studied the effects of the oxide during the FSE of A6061 aluminium tubes. Behnagh et al. [19] proposed a double-step tube production via FSE and implemented a numerical model to study process mechanics. However, in the considered papers a homogenization and/or used pre-compaction step is needed on the chips before applying the FSE process, increasing the energy consumption of the whole process and partially losing its advantages over conventional recycling routes. It is worth noting that tubes can also be produced by other solid state severe plastic deformation (SPD) techniques, such as accumulative spin bonding [20], tube channel pressing [21], high-pressure tube twisting [22], and tubular channel angular pressing [23]. Whalen et al. [24] turned AA6063 industrial scrap into consolidated tubes by applying a shear-assisted extrusion, studying the integrity of the different extruded profiles. Unfortunately, when SPD processes are employed for tube production, they require substantial amounts of energy. On the other hand, FSE is a promising candidate for sustainable tube manufacturing, as it potentially can require less time compared to other processes by directly turning chips into extruded tubes. However, the effectiveness of the process applied directly to the chips, in terms of mechanical and microstructural properties of the produced tubes, is yet to be proved. As a matter of fact, limited research was done on FSE process, and most researchers first turned chips into compacted billets used as workpieces for the actual extrusion of the tubes [19] or started from a bulk material [25–27].

The present research aims to produce friction stir extruded tubes directly from AA2024-O chips, in order to further strengthen the environmentally sustainability performance of such process category. The objective is to directly convert machining chips into consolidated aluminium tubes, eliminating any homogenizing or pre-consolidation steps, reducing energy consumption, and maintaining high product quality. Both experimental and finite element analysis approaches were utilized to examine the process parameters' effects on the mechanical and microstructural properties of the tubes produced via FSE. The main aim of the present research is to prove that tube can be obtained from chips with one single process step. Subsequently, mechanical and microstructural characterization is provided to correlate process parameters with tube quality. Numerical simulations have been implemented for analyzing field variable trends and justifying experimental grain size and hardness observations. Finally, the energy efficiency of the proposed approach is proved by measuring its electrical energy demand and comparing it with a more traditional two-step approach. Overall, this study lays the ground for expanding the solid-state processes recycling approach towards a wider industrial applicability.

## 2 Material and method

This study explores the potential of FSE of tubes made from AA2024-O aluminium chips. The chips produced had an average length ranging from 3.5 mm to 3.8 mm, a width of approximately 1.5 mm, and a thickness of 0.1 mm. To remove surface contaminants and any residual machining oil, a cleaning procedure was performed in accordance with

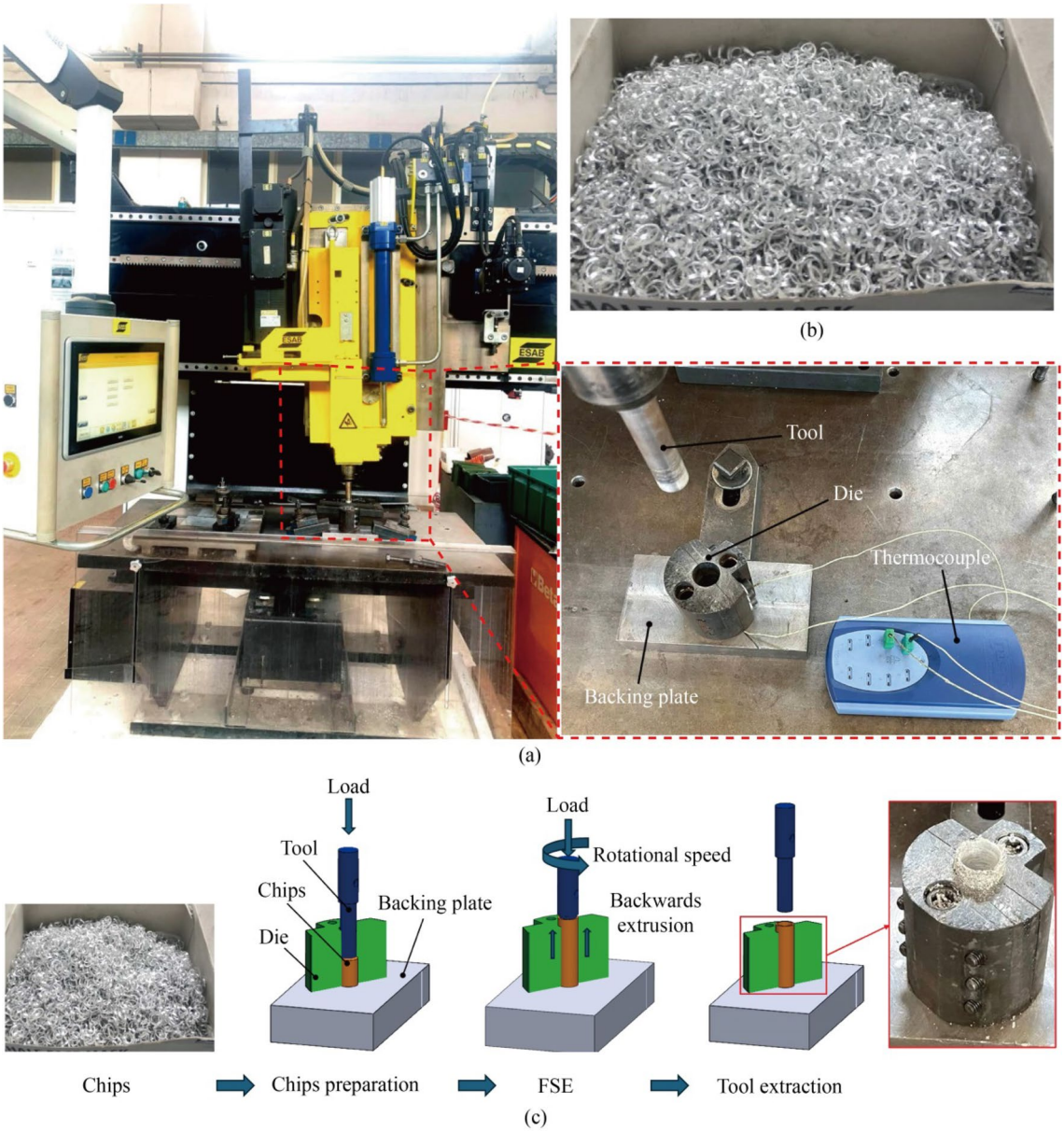


**Fig. 1** **a** Esab Legio machine for FSE tube extrusion, **b** aluminium chips used for the experimental campaign, **c** schematic diagram of the process

the ASTM G131-96 standard, utilizing acetone for degreasing chips. Moreover, a numerical analysis was conducted to examine the evolution of strain and temperature throughout the process. Lastly, the power required by the process was measured to assess the energy consumption of the FSE technique.

### 2.1 Experimental campaign

The experimental campaign was carried out using the ESAB LEGIO friction stir welding machine, which allowed force-controlled tool movement. The aluminium chips were obtained through a milling process performed on an AA2024-O aluminium bar. A fixed mass of 40 g of chips was loaded into the die chamber, which had an inner diameter of 25 mm and a height of 76 mm. Two H-13 steel tools were employed for the operation: one with a diameter of 25 mm for compacting the material and another with a diameter of 22 mm for extrusion. The complete experimental setup is shown in Fig. 1.

The FSE process for tube extrusion consists of two stages: chip preparation and extrusion process. At the first stage, the chips were pre-compacted up to 35 kN force using a compacting tool in order to adequately fill the die and avoid the

**Table 1** Set of process parameter combinations and ID name

| ID | Rotational speed/ ($r \cdot min^{-1}$) | Vertical load /kN |
|---|---|---|
| C1 | 1 000 | 12 |
| C2 | 1 000 | 15 |
| C3 | 1 000 | 18 |
| C4 | 1 500 | 12 |
| C5 | 1 500 | 15 |
| C6 | 1 500 | 18 |
| C7 | 2 000 | 12 |
| C8 | 2 000 | 15 |
| C9 | 2 000 | 18 |

dispersion of chips during the extrusion process. Moreover, the 35 kN compaction did not affect the extrusion process or the produced tube, but it was required to prepare the material for the extrusion stage. After this compaction phase, the compaction tool was replaced by the extrusion tool. In the second stage, the extrusion process is run by varying the process parameters as shown in Table 1. At the beginning of the extrusion process, the vertical force gradually increases by 0.5 kN/s from 5 kN to reach the maximum required force for the assigned processing conditions. At the end of the extrusion process, the tool automatically reached its initial position and the tube was extracted. It is worth remarking that a similar setup has been adopted by Behnagh et al. [19] and Whalen et al. [24] for extruding tubes (from machining chips) via double step friction stir consolidation and ShAPE process, respectively. In both cases, a rotating tool and a designed die were employed in the process setup.

In order to observe the variation in temperature at various processing conditions, a K type thermocouple was placed into a hole drilled at 1/3 of the height of the die (from the bottom), 1 mm before the inner die wall (see Fig. 2a). As reported in Table 1, the experimental plan included three different values of tool force (12 kN, 15 kN, and 18 kN) and rotational speed (1 000 r/min, 1 500 r/min, and 2 000 r/min). Each test combination ("Ci") was run three times to ensure the reliability and consistency of the results.

Temperature monitoring was crucial to prevent the tube tool from sticking, which could result in damaging the machine and the tube itself, therefore the process stopped when the tool displacement reached almost 35 mm which, from the experimental campaign, corresponded to a measured temperature in the range of 370–380 °C. This range of the die's temperature can be assumed as the limit temperature of the setup proposed.

The selection of these parameters was guided by previous studies on the FSC and FSE process. Since the optimal parameters for achieving sound bonding were identified as 1 500 r/min and 15 kN, a variation range of ±500 r/min was

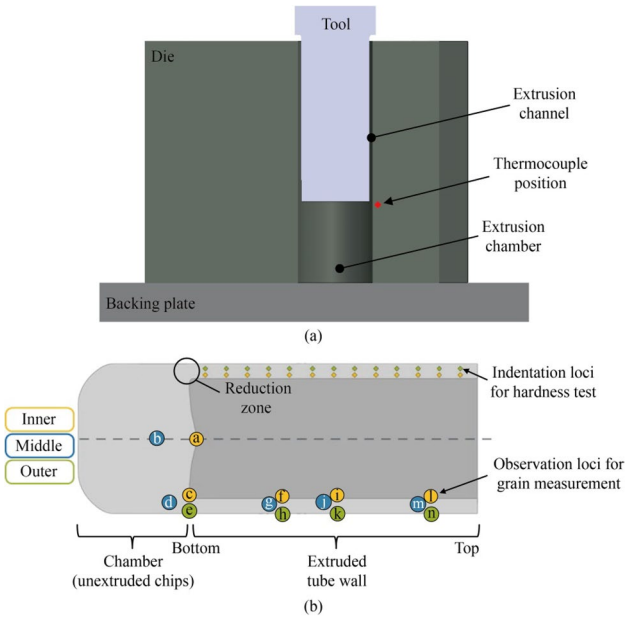


**Fig. 2** Detailed view of **a** the experimental setup section and **b** longitudinal section of the billet

adopted to investigate the influence of temperature input on tube production.

Specimens were extracted from each extrudate to assess the material properties through mechanical and microstructural analyses. The specimens were prepared by mounting, polishing, and etching using Keller's reagent, composed of 2 mL HF, 3 mL HCl, 5 mL $HNO_3$, and 190 mL $H_2O$. Concerning the microstructure analysis, the grains were studied along the longitudinal section identifying three loci along the radius of the tube, specifically near the outer surface, at the middle of the tube, and near the inner surface as shown in Fig. 2b (letters). The grain size was measured by using a GX51 Olympus optical microscope with 100× lens and evaluated following the ASTM E112-96 by the ImageJ software. For microstructural analysis, an SEM equipped with EDS was used to investigate defects within the tubes, surface characteristics, and material composition.

For mechanical analysis, Vickers microhardness testing was conducted along the longitudinal section of the tubes, spanning from the inner to the outer surface, in compliance with ISO 6507 standards. A load of 5 N (0.5 kg) was applied for 15 s. This procedure provided insights into the material's localized hardness gradients as shown in Fig. 2b (points). To evaluate ductility and structural integrity, compression and flattening tests were systematically performed. The flattening test involved radial-axis compression of tubular specimens using a tensile testing apparatus. This method, aligned with ISO 8492 guidelines [28], enabled the assessment of radial deformation capacity and stress-strain behavior under controlled loading. For this study, specimens measuring 15 mm

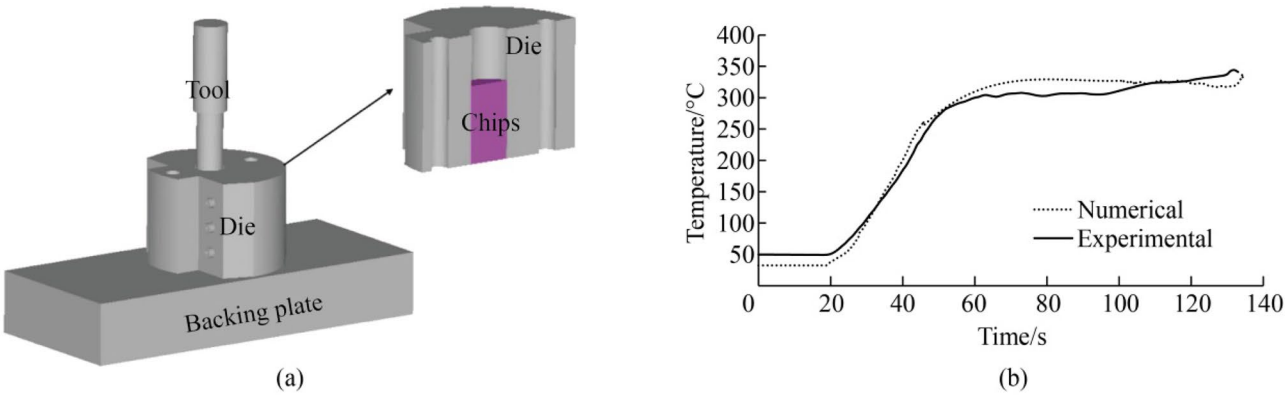


**Fig. 3** **a** Numerical setup of the FSE of tubes and **b** temperature tuning of numerical and experimental tests

in width were extracted from the extruded tubes and subjected to flattening tests. The quasi-static lateral compression tests were performed in compliance with AS 2505.3–2004 and ISO 8492 standards, utilizing a universal tensile testing machine. The top plate was moved at a constant rate of 0.05 mm/s until reaching the maximum displacement of 20 mm. Force and displacement data were recorded at a sampling frequency of 10 Hz.

Lastly, an ARNOUX CHAUVIN C.A. 8331 analyser was employed to monitor voltage, current, and power profiles during operation. This device facilitated precise measurement and comprehensive evaluation of power absorption trends.

### 2.2 Numerical campaign

The numerical investigation of the tube production process was conducted using the commercial finite element software SFTC DEFORM 3D. Mirroring the experimental approach, the numerical model incorporated four key components, as illustrated in Fig. 3a. Three of these components—tool, die, and backing plate—were modeled as rigid bodies made of H-13 steel, with mesh resolutions of 60 000, 60 000, and 30 000 elements, respectively. The aluminium chips were represented as a compressible rigid-viscoplastic porous billet. The initial relative density of the billet was analytically determined to be 0.7 based on the die chamber volume (25 mm diameter × 76 mm height) and the mass of the loaded chips (40 g). Additionally, a mesh window (reduction of 30%) was employed close to the bottom of the tool to better investigate the field variable in this critical zone.

A calibration procedure was performed for the 1 500 r/min and 15 kN case to identify the optimal shear factor by comparing numerical and experimental temperature profiles (see Fig. 3b). This tuning approach, already validated in Refs. [29, 30], aimed to vary the thermal coefficient until adequate matching was observed. As result of the temperature tuning procedure, a shear factor of 0.2 and interface heat transfer coefficients (IHTCs), of 11, 45, and 45 W/(mm$^2$·K) for the billet-tool, billet-die, and billet-backing plate interfaces were selected. The process parameters applied during the experimental campaign served as input variables for numerical characterization.

## 3 Results and discussion

### 3.1 Mechanical characterization

For evaluating the mechanical properties of the extruded tubes, microhardness tests were conducted along the longitudinal section with equally spaced indentations. The hardness measured at the corresponding observation loci is highlighted in Fig. 2, and the resulting average hardness values are plotted in Fig. 4. The hardness value increases with the increase in processing parameters. The maximum hardness value of 147 HV was observed for the sample C8, resulting in a 140 % increase (from 61.5 HV to 147 HV) compared to the AA2024-O base material. This huge improvement in hardness was in accordance with what was revealed by Baffari et al. [31] on AA2050 aluminium friction stir extruded wires. In this respect, Baffari et al. [31] observed that the hardness of the produced AA2050 wire via FSE was close to the hardness of the AA2050 at T3 condition.

The same phenomenon happened here. In fact, the hardness of AA2024-T3 is about 137 HV which is very close to the hardness acquired and shown in Fig. 4. Overall, the hardness increases with increasing the vertical force. Such an effect is more visible when passing from 12 kN to 15 kN. The impact of force increasing on hardness is less visible when moving from 15 kN to 18 kN. For the ID C9 even a slight decreasing trend is visible. This phenomenon is related to excessive heat, i.e., high force and rotation speed, which results in hot cracks formation and surface melting.

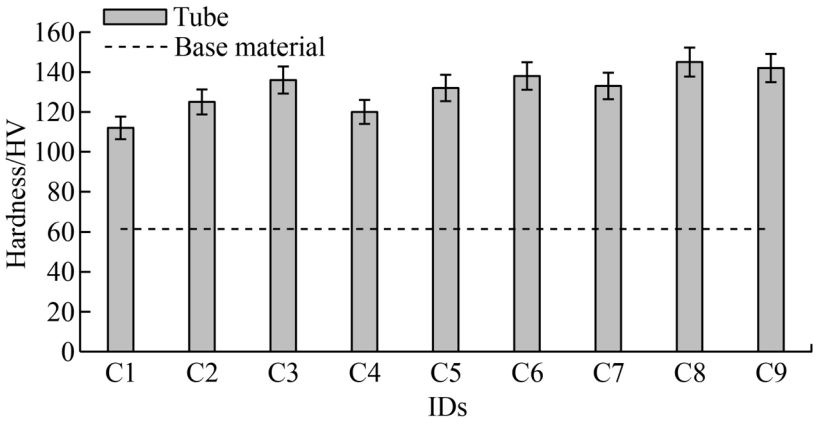


**Fig. 4** Hardness results of the extruded tube for the 9 cases' study (longitudinal section)

On the other hand, the lowest hardness is observed at ID C1, which in this case is due to low heat input, resulting in weak consolidation and porosity formation phenomena. Regardless of the processing parameters, the overall hardness value increased with respect to the base material.

To evaluate the deformation behavior of the produced aluminium tubes, compression tests were conducted. In these tests, the cross-section of the tube was compressed among two flat, parallel, and rigid plates. As the top platen descended, initial contact with the tube occurred at discrete points, as illustrated in Fig. 5a. With the increase of the load, the contact regions began to flatten against the plates, causing the tube to deform showing barreling phenomena until reaching its elastic limit. Upon exceeding the elastic limit, two plastic hinges were formed (see Fig. 5b), until fracture occurred, causing a load drop. The load-displacement curves for the three case studies at various rotational speeds (1 000, 1 500, 2 000 r/min) and under a constant extrusion force of 15 kN, are shown in Fig. 5c. From the graph it shows that the specimen ID C5 represents the maximum compression stress compared to IDs C2 and C8 rotation speed specimens. The high compression stress in sample ID C5 indicates successful chip bonding and fewer cracks or less porosity formation (see Sect. 3.2). Interestingly, similar average hardness values were reported in tube manufacturing via FSE of aluminium powders by Baffari et al. [32]. In particular, they observed an increase in hardness with increasing feed rate, with values in the range of 130–140 HV, consistent with the results shown in Fig. 4.

Flattening tests were also performed and force-displacement curves for tube samples were plotted (see Fig. 6c). As well as for the compression test, the case study ID C5 showed the highest mechanical properties, reflecting high flattening stress and effective bonding between chips. On the other hand, IDs C2 and C8, which observed porosity and hot cracks, showed lower mechanical behavior as it would be better explain in microstructural analysis part.

The results on global mechanical properties derived for compression and flattening test can be explained by looking at local defects that will be also discussed in Sect. 3.2. Overall, it was possible to state that the increase of tool's rotational speed, i.e., ID C9, resulted in the formation of hot cracks and increased surface roughness; insufficient heat generation at low rotational speed, i.e., ID C1, might result in a lack of consolidation and porosity occurrence.

### 3.2 Microstructural analysis

In the cross section, different acquisitions were performed to characterize the evolution of the grain size along the radial direction (see Fig. 7). Results showed that the outer and inner regions of the tube were characterized by smaller grain size compared to grain size of the middle region. This phenomenon is due to the tool stirring action creating severe plastic deformation and frictional heat, therefore the dynamic recrystallization occurs and produces a fine-grained structure especially in the inner surface. Concerning the outer region, the limited grain size is due to the external roughness that inhibits the grain growth [31, 32]. In this regard, the average grain sizes measured for the case study ID C5 were 3.5 μm, 4.4 μm and 3.4 μm for the outer, middle and inner regions (see Fig. 7), respectively.

An overview of the longitudinal grain size evolution was performed by considering the observation loci reported in Fig. 2b. The selected observation loci provide a complete view of the grain evolution moving from the billet to the wall thickness; therefore it is possible to describe the "story" (evolution of the grains) of the material, from the unextruded chips to the extruded tube's wall. Results for case study IDs C2 and C5 are reported in Fig. 8. The grains acquired just under the tool (positions A and B) were subjected to a thermal coarsening due to the heat and a low level of strain (around 6 μm); close to the extrusion channel (C and D), material flow had the effect of elongating the grain (around 8–10 μm) along longitudinal direction. Before extrusion,

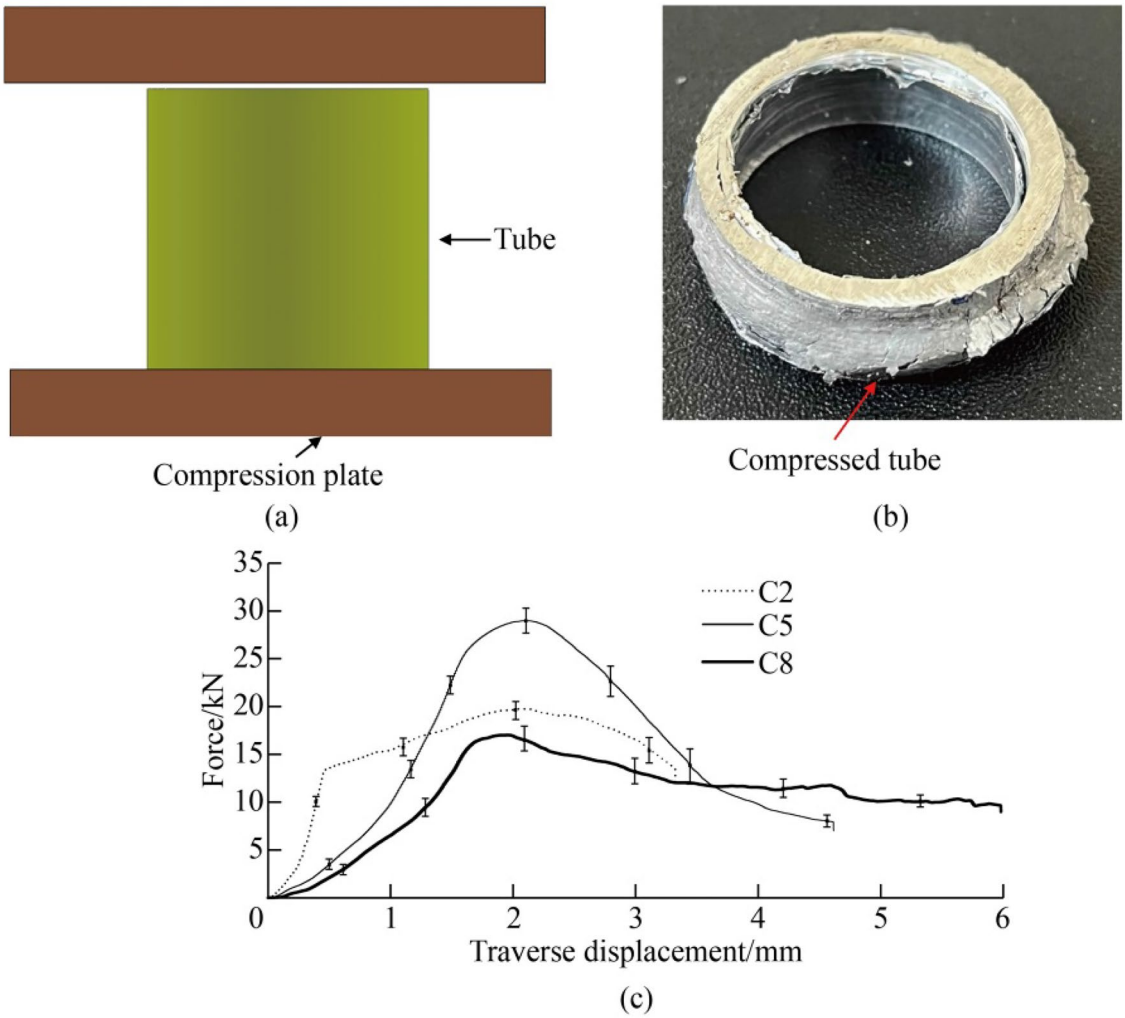


**Fig. 5** **a** Schematic fixture used for compression test of tubes, **b** compressed tube for the case study ID C5, **c** compression test results at three case studies (IDs C2, C5, and C8)

the material undergoes a consolidation mechanism similar to the friction stir consolidation (FSC). In fact, the range of grain size values was in accordance with what found by Puleo et al. [29]. On the other hand, the material within the extrusion channel underwent high pressure and deformation, showing refined grain size (around 4 μm). After passing through reduction zone, the grain size remains essentially unchanged along the tube walls (from zone E to zone H).

It is worth mentioning that points C and D show bigger grain size for case study IDs C5 than C2 mainly because of the different heat conditions. Specifically, the increase in rotational speed led to an increase in temperature [33], which promoted grain growth. When the material reaches the extrusion channel, a refining process starts (as mentioned before), but the effect of increased grain size remains visible along the longitudinal section of the tube. By comparing the microscopic and macroscopic analyses it is clear that the hardness results (see Fig. 4) are consistent with the microstructural evolution shown in Fig. 8. In particular, the fine and equiaxed grains observed for the C5 condition are correlated with the increased hardness values measured at the same process parameter. In Fig. 8c, the porosity analysis of the extruded tubes for case study C5 was conducted using optical microscopy. The results indicate a porosity of 1.94 %, which is relatively low under appropriate rotational speed and extrusion force conditions. This reduction in porosity can be attributed to effective material plasticization achieved at the optimized process parameters, resulting in improved mechanical performance and enhanced microstructural integrity. Similar porosity values have also been reported by Huda and Zaharinie [35] in the extrusion of wire.

Lastly, the AA2024 tubes were sectioned in the longitudinal direction for microstructural evaluation by SEM. Through-thickness micrographs of the tube wall are shown in Fig. 9. For the case study C1, low heat input, i.e., low tool force and rotation is shown in Figs. 9a and b. This is due to

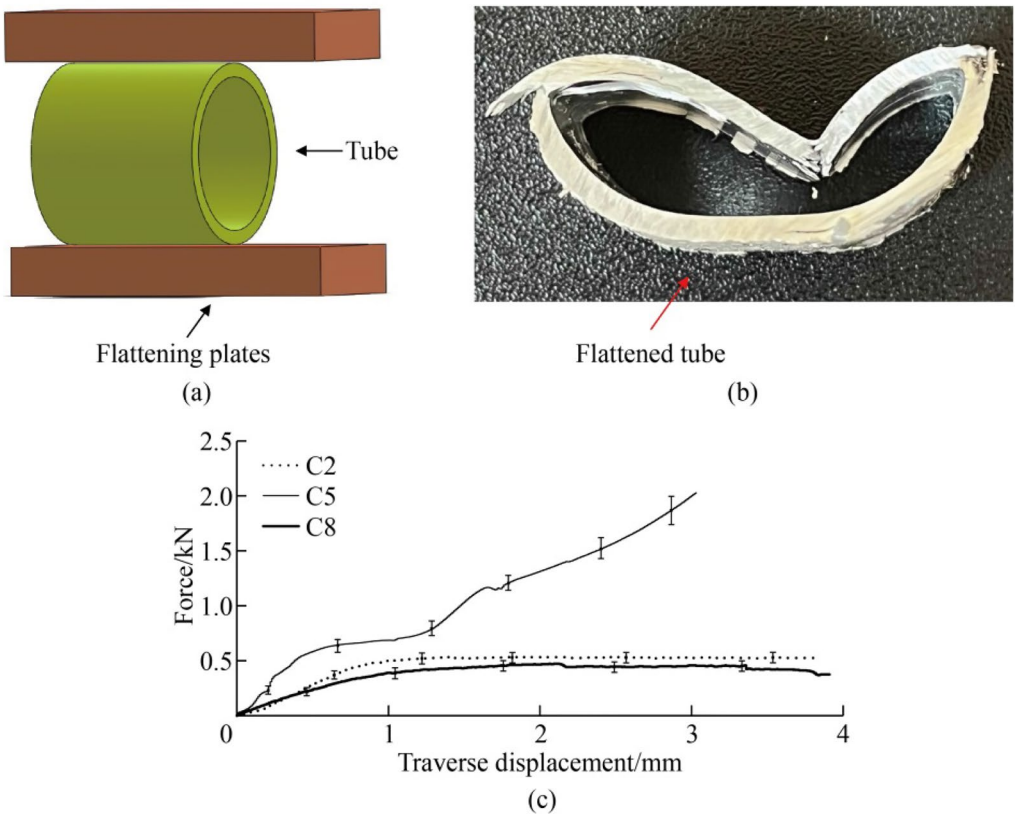


**Fig. 6** **a** Schematic fixture used for flattening test of tubes, **b** flattened tube for ID C5, **c** flattening test results in three case studies (IDs C2, C5, and C8)

insufficient heat for the chips to plasticize and bond. While at optimum rotational speed and force for the case study C5, the SEM image of the cross-section of the AA2024 tube is shown in Fig. 9c. The specimen exhibits a nearly uniform material flow, and a good bonding between aluminum chips has been observed, which causes improvement of properties and reduced porosity. This is due to the sufficient heat provided by tool rotational speed and sufficient extrusion force causing the extruded material to bond properly, which results in defect-free extruded tubes. The EDS mapping and analysis of the corresponding case study are shown in Fig. 9d. These results are in accordance with the main findings concerning global mechanical properties discussed in Sect. 3.1.

### 3.3 Numerical results

The numerical simulation is used to provide insight into the process' mechanics and motivate the observed experimental results. The first phenomenon here discussed is the change in grain size along radial direction. In Fig. 10, the effective strain distribution across the cross-section of the tube for case study C5 is reported. It is interesting to notice that the recrystallization behavior, previously highlighted in Fig. 7, is corroborated by the effective strain evolution along the radial direction predicted by numerical simulation; the internal section of the tube (directly in contact with the tool) undergoes higher strain than the external or middle one, resulting in better grain refinement.

Additionally, the evolution of the effective strain from the beginning of the process to the end is depicted in Fig. 11. In this figure, two main phases were identified to better describe the curves: transition phase and steady state phase. In this phase, the material enters the clearance between tool and die, i.e., the reduction zone; and thanks to high deformation levels (see strain rate in Fig. 12), it is forced to extrude. Once the material reaches the extrusion channel, the strain level remains almost unchanged.

A more specific explanation of the grain size distribution along the thickness of the tube has been provided by studying the Zener-Hollomon parameter ($Z$) (see Fig. 12). It is known that the average grain size decreases with decreasing of the working temperature and increasing of working strain rate ($\dot{\varepsilon}$) [34]. According to the Zener-Hollomon formulation (see Eq. (1)), the average grain size decreases when the strain rate increases or the temperature decreases.

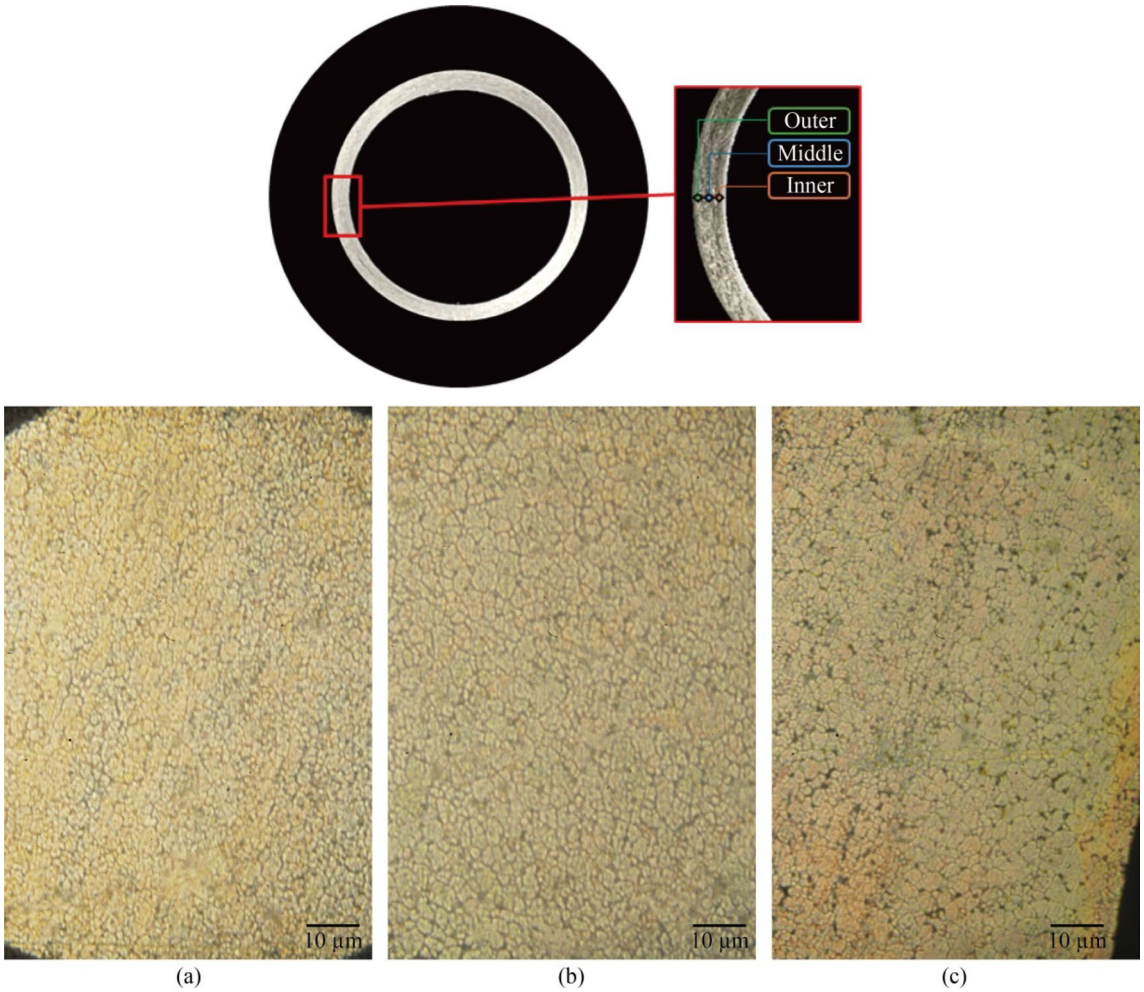


**Fig. 7** Microstructure analysis of the cross section of the case study ID C5 tube **a** outer, **b** middle, and **c** internal surface

$$Z = \dot{\varepsilon} \exp(Q/RT), \tag{1}$$

where $Q$ is the activation energy [35]; $R$ is the constant of the gas; and $T$ is the absolute temperature (K).

Considering as an example the case study C5, in Fig. 12, temperature, strain rate and logarithmic Zener-Hollomon (Log$Z$) parameter are plotted for 40 s processing time. This figure shows that the temperature increases near the reduction zone, where the material undergoes high levels of deformation. The combination of high strain rate and temperature resulted in a low value of the Zener-Hollomon parameter, which was index of big grain size (see Eq. (1)).

In Fig. 13, a detailed view has been proposed by varying the scale value of the $Z$-parameter. Specifically, in this figure, the upper bound and lower bound of the scale were set to catch the small variation of the $Z$-parameter along the thickness. The results showed an increase at the external surfaces (namely internal and external) while decreasing towards the center of the tube (see Figs. 13a, b).

### 3.4 Limit of the process: extrusion velocity reduction

In Fig. 14, the comparison between three different temperature-tool displacement curves has been presented aiming to describe the limit of the process. Specifically, three case studies were selected to describe the effect of different rotational speeds (IDs C2, C5 and C8) on tube extrusion.

Firstly, looking at the shape of the tool displacement curve for case study ID C2 (see Fig. 14a), it is possible to note a linear trend. This means that the extrusion rate is quite constant. When looking at the tool displacement trend of case ID C5 (see Fig. 14b), a different behavior is recorded, instead. Specifically, an initial linear trend is visible, at 40

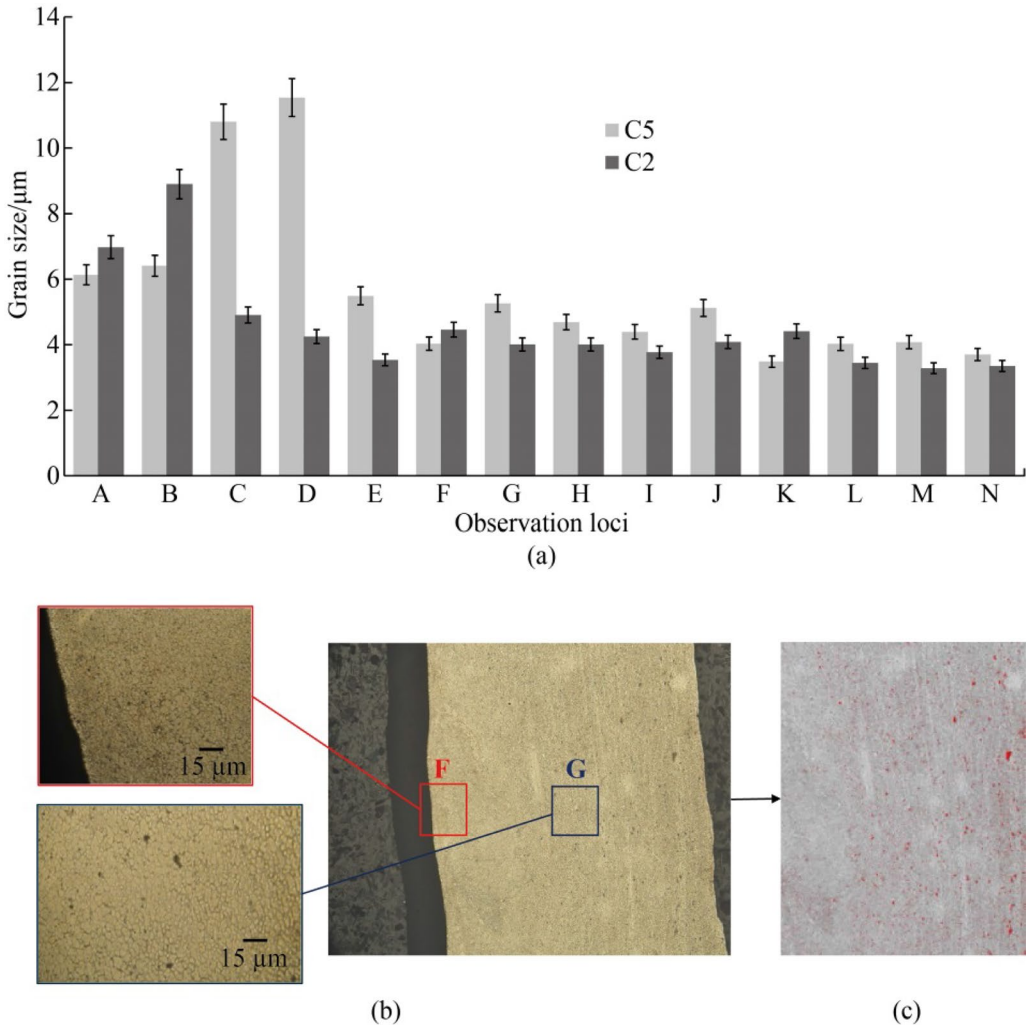


**Fig. 8** **a** Grain size distribution along the longitudinal section for C5 and C2, **b** tube longitudinal section of C5 and **c** porosity evaluation image

s processing time a slope change occurs, proving an extrusion rate decrease. This phenomenon is even more visible in Fig. 14c, where the displacement and temperature trend for case study ID C8 are reported. From this observation, it is possible to state that the process reaches a sort of stuck condition when high temperatures are reached. Actually, for all the tests, the temperature peak was close to 350 °C but it was reached at different process times, while the maximum displacement was almost the same.

This might appear counterintuitive, as an increase in temperature causes material softening, and thus the extrusion conditions should be eased. Nevertheless, this phenomenon is to be attributed to the consolidation level of the unextruded chips still in the extrusion chamber rather than to the temperature enabled softening effect. In fact, the increase in temperature eases the solid bonding occurrence of the material still present in the extrusion chamber. As a given level of consolidation is reached, the extrusion conditions worsen as a higher vertical load should be applied to keep the extrusion rate constant. Moreover, the faster the temperature increases, the faster the material consolidates, and the earlier the extrusion rate reduction phenomenon occurs (ID C8, see Fig. 14c). A comparison of the temperature profiles for C2, C5 and C8 is proposed in Fig. 14d, to better visualize the heating effect of different rotational speeds at the same load. In this figure, it is clear that higher rotational speed leads to greater temperature increasing rate, resulting in both excessive consolidation and early process termination.

Figure 15 shows the temperature distributions obtained at different rotational speeds within the same process window. It is clearly visible that higher rotational speeds (see Fig. 15c, ID C8) lead to increased temperatures, particularly near the extrusion channel. This behavior promotes faster material consolidation, but possibly resulting in an earlier process interruption.

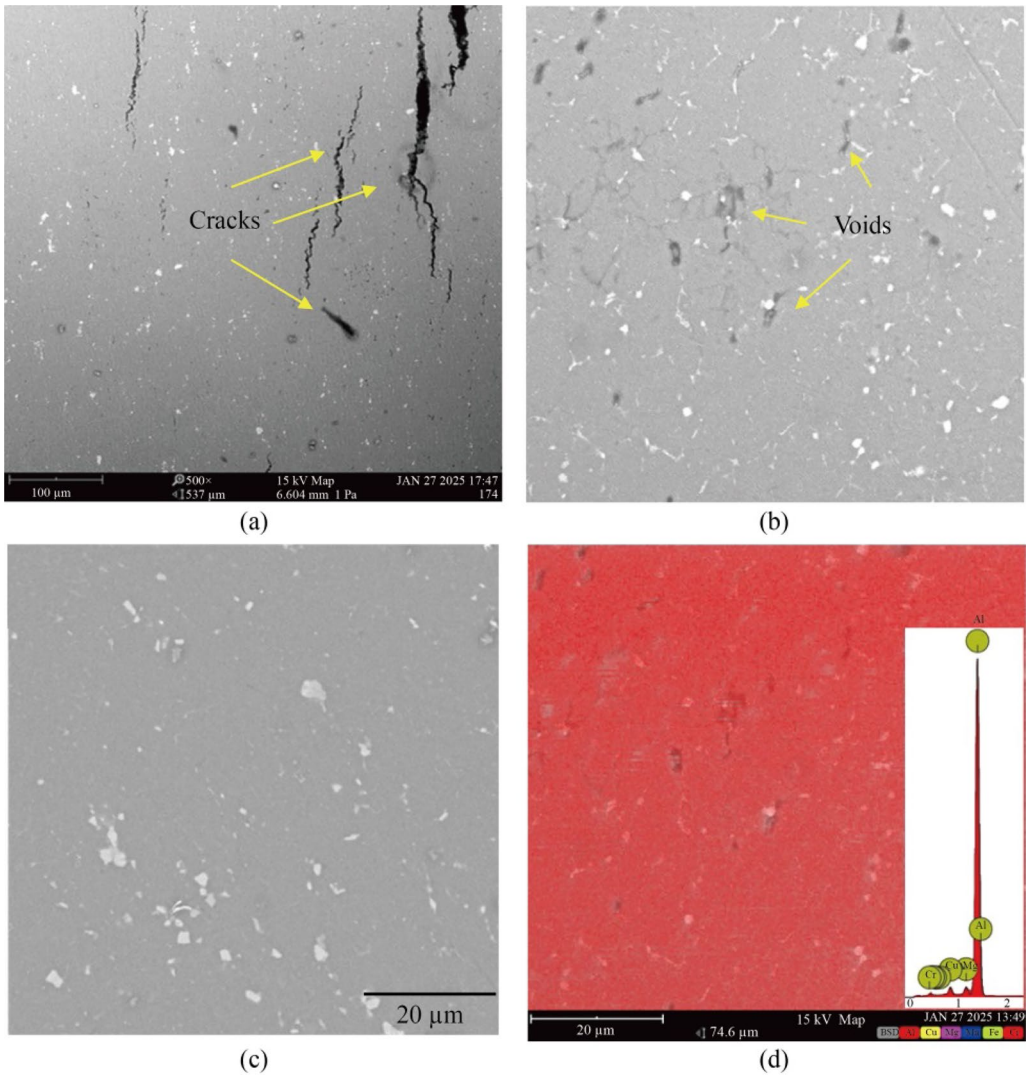


**Fig. 9** **a, b** SEM images of the cross-section of the sample ID C1, **c** SEM image of the cross-section of the sample ID C5, **d** corresponding EDS mapping and analysis

For a better understanding of the phenomenon, the density evolution during the process has been numerically analyzed and the results for case study ID C5 are reported in Fig. 16. It is possible to notice that the portion of the unextruded chips in the extrusion chamber reaches density equal to 1 as the processing time increases. After 60 s, the entire sample is almost all at density equal to 1.

To further support this finding, solid bonding occurrence was investigated in the material chamber zone. The aim was to study the consolidation occurrence for the material located at the bottom of the extrusion chamber (not extruded material) during the tube extrusion process. This study was carried out by analyzing the bonding condition with varying the processing time over a set of 119 observation loci, as reported in Fig. 17a. For monitoring the bonding condition, the Donati and Tomasini criterion was used [36], as it was specifically tuned on extrusion process. With such kind of approach, the bonding value $W$ in a given observation loci is calculated using stress and strain values extracted from the numerical simulation, then the value is compared with a limit value $W_{\text{lim}}$. When the bonding value of a point is greater than the corresponding bonding limit value, that point is considered as consolidated. $W_{\text{lim}}$ value changes with material and temperature, and proper bonding limit values should be identified for the used material and the recorded process temperatures. In this regard, the $W_{\text{lim}}$ expression reported in Eq. (2) was used; this expression was calculated

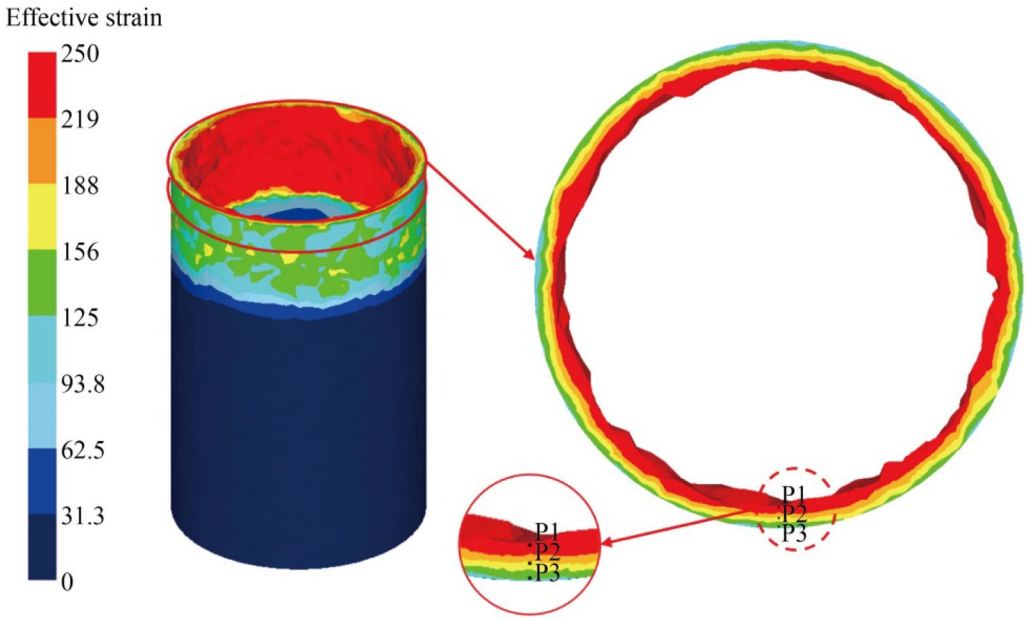


**Fig. 10** Strain plot in the circumferential section of the tube, case study C5

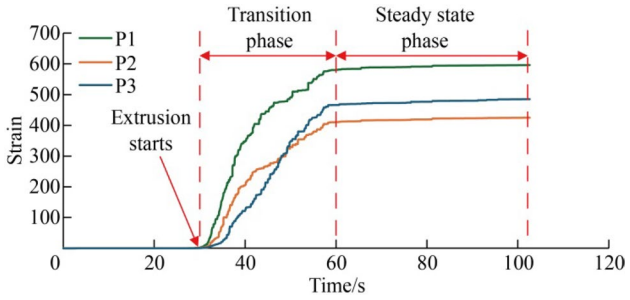


**Fig. 11** Strain evolution of the three loci: internal (P1), middle (P2) and external (P3) for the case study C5

using the data for the AA2024 and the related approach presented by Puleo et al. [29].

$$W_{\text{lim}} = -1 \times 10^{-4} T + 0.0653. \tag{2}$$

Bonding conditions were evaluated at different process times windows, namely 40, 50, 60 and 70 s, the results are reported in Figs. 17b–e.

The bonding maps in Fig. 17 revealed that the consolidation phenomenon already began at 40 s. As the process time increased, the consolidation front moved downward, resulting in almost complete material consolidation at around 70

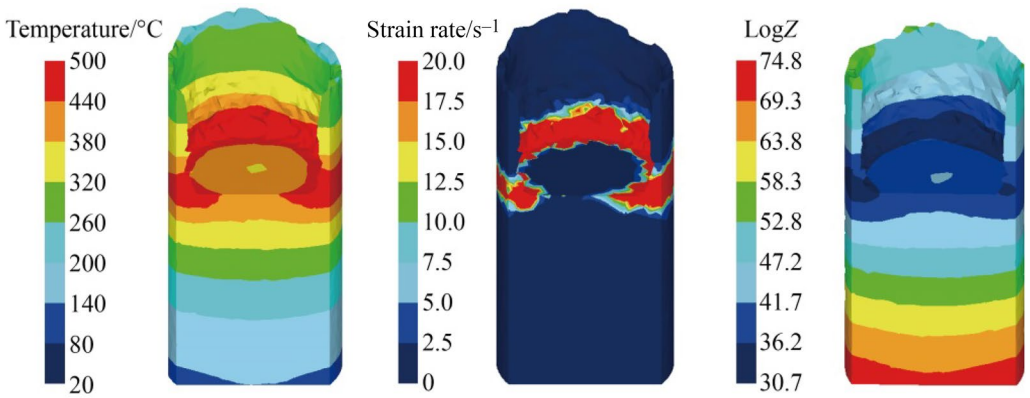


**Fig. 12** Temperature, strain rate and log$Z$ distribution at 40 s for the case study C5

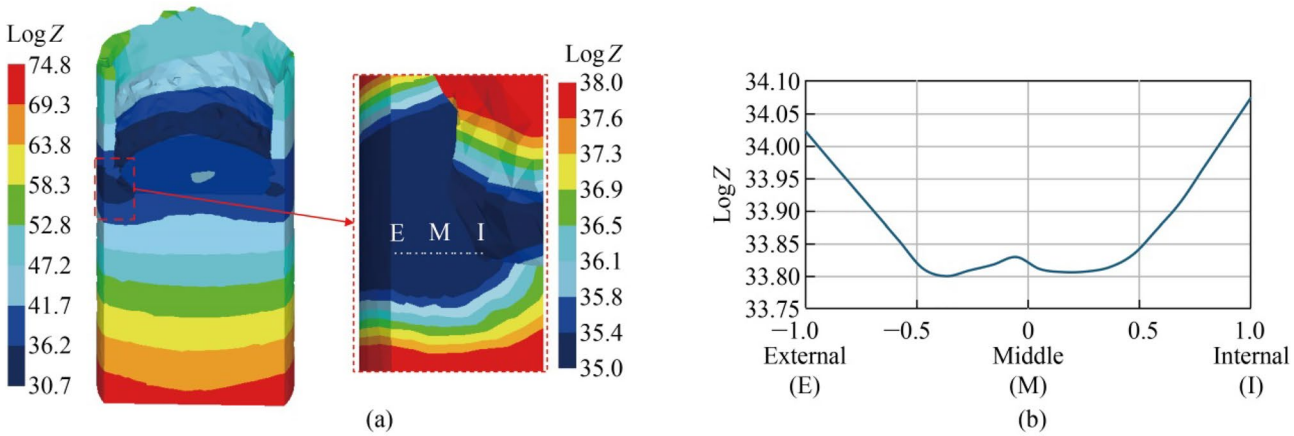


**Fig. 13** **a** Zener-Hollomon parameter distribution at the extrusion channel, **b** Zener-Hollomon analytical distribution along the external (E), middle (M), and internal (I) surface of the extrusion channel

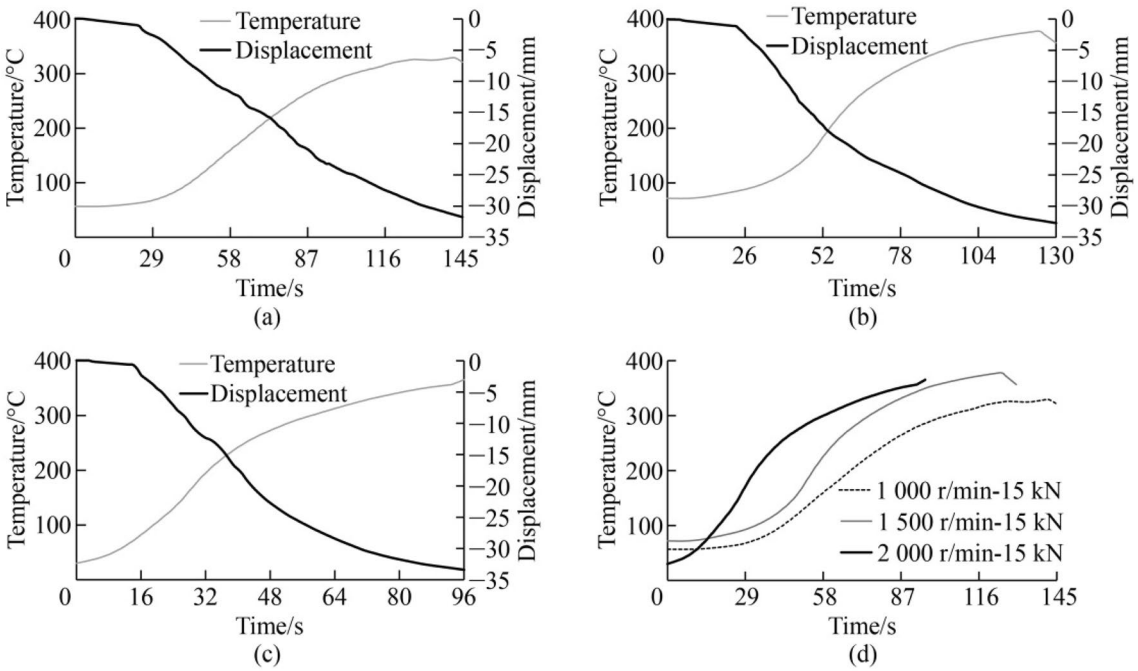


**Fig. 14** Temperature versus displacement graph **a** C2, **b** C5, **c** C8 case studies, **d** comparison of C2, C5 and C8 temperature profiles

s. This bonding condition analysis is consistent with what above reported concerning density and displacement trends.

As a result of this analysis, different approaches can be considered to mitigate the issue presented. Examples include the use of an active cooling system or, alternatively, a variable tool rotational speed. In the first case, the cooling system could be integrated into the die setup to control the material temperature at the bottom of the die, thereby promoting a slower consolidation of the unprocessed material. The second approach focuses on in-process control of the tool's rotational speed, combined with sensors and thermocouples. This would enable a real-time adaptive system that modulates the rotational speed (reducing the velocity if too hot or increasing if too cold) based on the heat input generated by the friction.

### 3.5 Electrical energy consumption results

One of the main novelties of the proposed approach concerns the possibility to turn chips directly into tubes by one single-step manufacturing approach. Actually, other approaches already presented are made of pre-consolidation

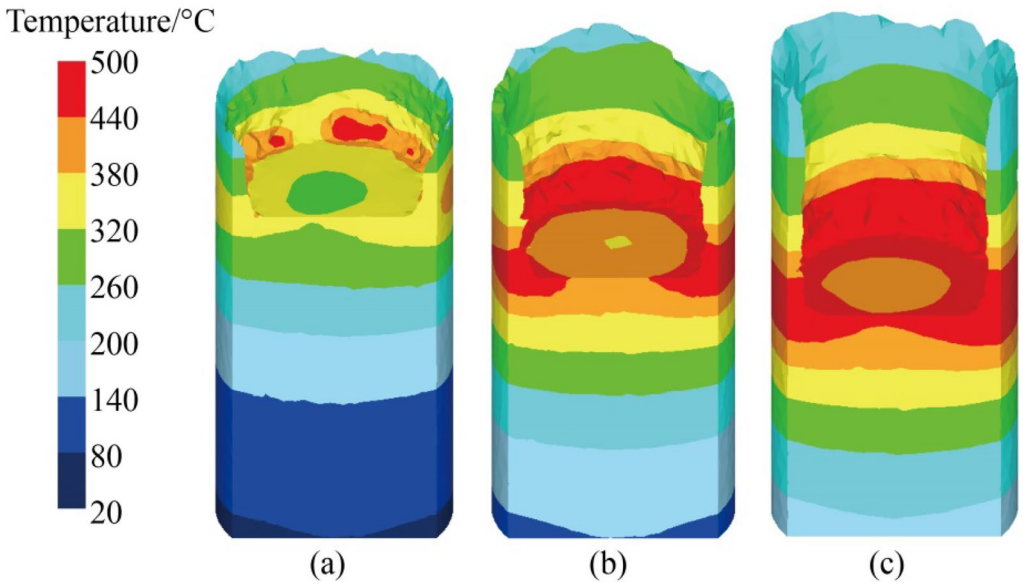


**Fig. 15** Temperature plots for the case study IDs **a** C2, **b** C5 and **c** C8 at the process time window (40 s)

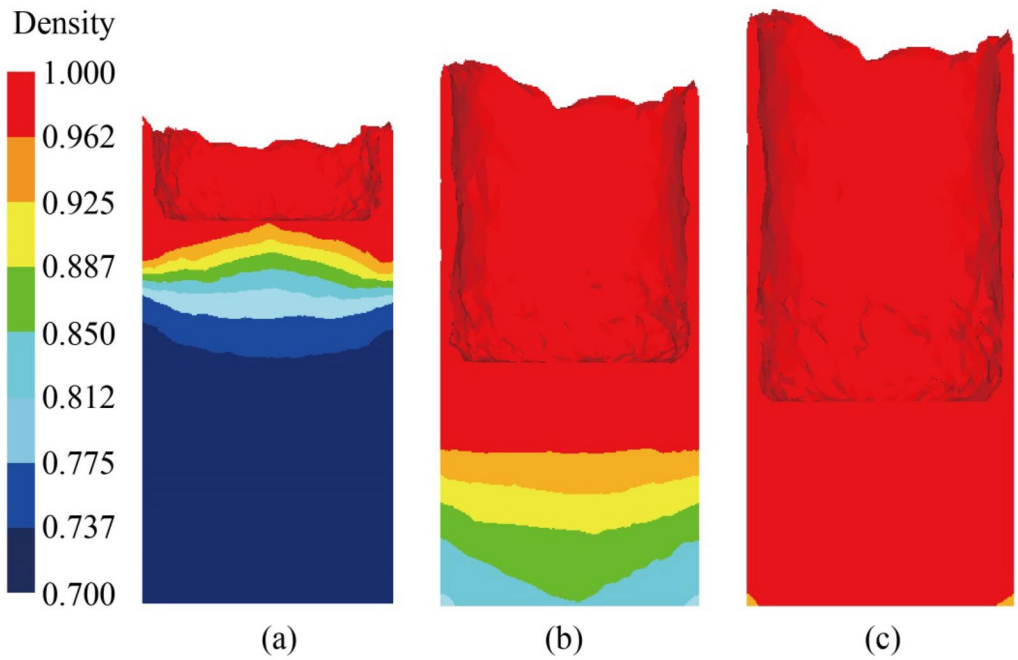


**Fig. 16** Density evolution of the case study ID C5 at **a** 30 s, **b** 50 s and **c** 65 s

and/or homogenization step prior to the extrusion process. The single-step nature of the FSE approach enables energy saving, further contributing to reduced environmental impact of aluminum-based products. In this section, the electrical energy characterization of tube production through FSE is provided and compared to that characterizes double steps approaches. The electrical energy was measured by means of a power and energy quality analyzer, Chauvin Arnoux C.A. 8331 (sampling rate of 12.8 kHz, results logged and shown are for averaged values over one second intervals) connected to the machine input. The entire working cycle was monitored from chips compacting up to tool withdraw. The typical power consumption profile is plotted in Fig. 18a. This figure depicts the power consumption of the entire process,

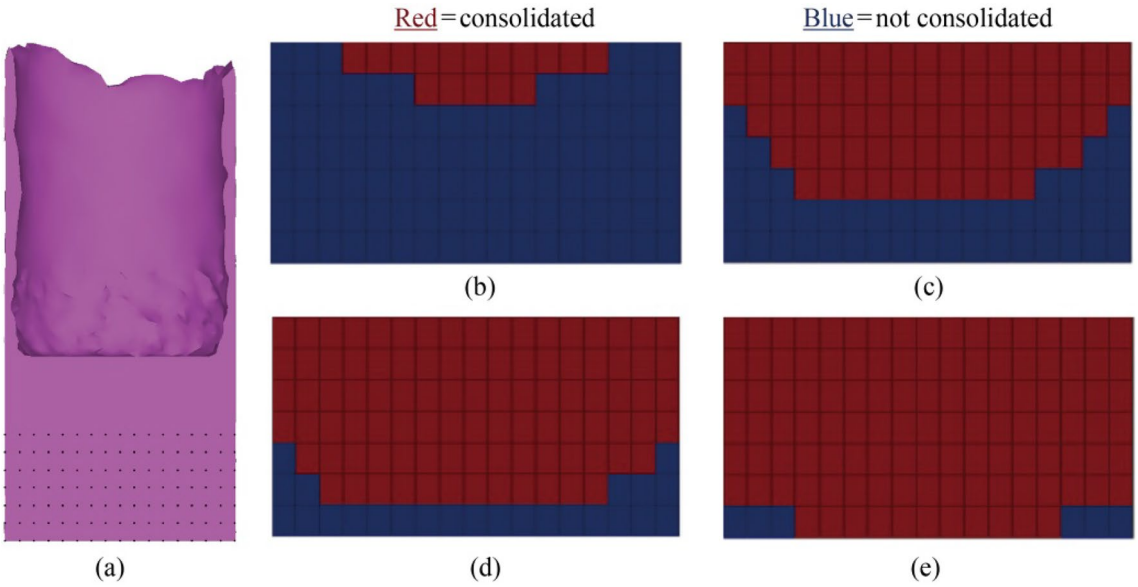


**Fig. 17** **a** 119 observation loci at the bottom of the cross section of case study C5 at 60 s; solid bonding occurrence maps **b** 40 s, **c** 50 s, **d** 60 s, **e** 70 s

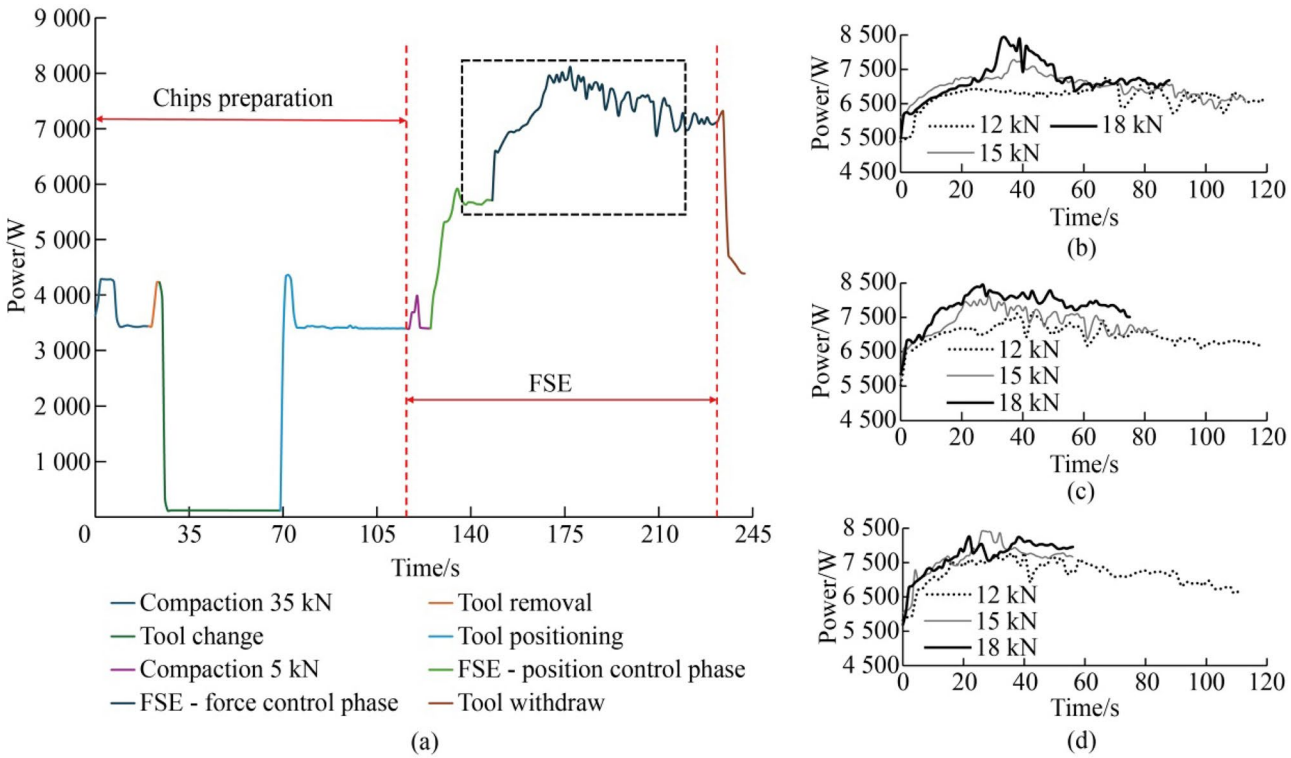


**Fig. 18** **a** Power consumption profile across processing phases and comparative analysis of the force control window (black dashed window) at **b** 1 000 r/min, **c** 1 500 r/min and **d** 2 000 r/min

starting from the cold pre-compaction at 35 kN (needed for ensuring to fill the extrusion chamber) up to the extrusion process. This process was carried out by switching from a position control phase to force control phase. The first one, position control phase, is a brief phase where the tool moves downward for a few millimeters (at 5 kN) to ensure adequate contact with the material. The second one, force control phase, is the actual extrusion process where the force

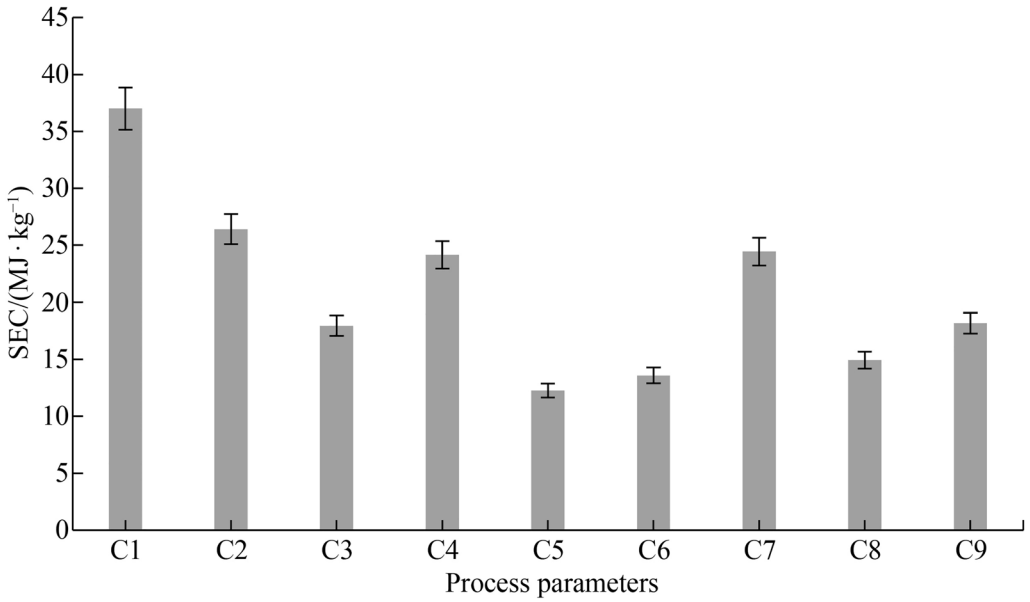


**Fig. 19** SEC evaluation for all the case study

increases from 5 kN to the required force (12 kN, 15 kN or 18 kN) and the tube is extruded. Moreover, the first part of the process, namely chip preparation, was the same for each test, while the second part, FSE, was characterized by a similar shape with different power levels depending on the process parameters used. The power absorbed by the machine was recorded and plotted against the process time for the three considered values of tool rotation (1 000 r/min, 1 500 r/min, and 2 000 r/min) (see Figs. 18b–d). It is noteworthy that variations in force have no significant impact on power consumption. However, the processing time decreases (and therefore the electrical energy consumed) with an increase in tool force and tool rotation. As previously discussed, this behavior can be attributed to reduced heat generation at lower rotation speed and force, which results in low extrusion rate and, consequently, long processing times.

From Fig. 18, it is visible that the power needed for the extrusion exhibits a starting increasing trend followed by a decreasing trend. The reason behind this phenomenon can be attributed to the material flow. Specifically, at the beginning of the process, the temperature increases due to the friction between the rotating tool and chips. When the material is plasticized and extrusion starts, the hot material extrudes leaving the cold one behind, which causes a decrease in temperature. At this point, less power is required for extrusion, resulting in a comparatively decrease in power.

A further investigation on specific energy consumption (SEC) was carried out to quantitatively assess the influence of different process parameters. The SEC evaluation was performed by considering the same height of tube produced, therefore the same mass, as functional unit. Specifically, the extrusion speed at steady state was employed to calculate the time required for extruding the fixed height of tube. Consequentially, the average energy absorbed was then divided by the mass to obtain SEC values. The results are summarized in Fig. 19.

From Fig. 19, it can be observed that the process duration has a stronger effect on SEC than energy consumption. In this regard, comparing the SEC results of 1 000 r/min samples and the process times (see Fig. 18b), it is clear that although the power required for extruding is lower for C2, the specific energy consumption is the highest due to the process duration. When the process time is reduced, the SEC is lower as demonstrated for C4 and C7. Additionally, the energy plays a significant role for tests with comparable process time (C5 and C6 or C8 and C9). In these scenarios, the higher the energy, the higher the SEC. Lastly, concerning the comparison among C2, C5 and C8 which was proposed in different chapters, it was evident that both tube quality obtained in C5 and the lower SEC led to regard this parameter combination as the optimal solution.

When compared to the conventional remelting process, the efficiency of this approach becomes evident. Cooper et al. [37] reported that the total primary energy required for chip recycling (melting), recovery of melting losses (10%

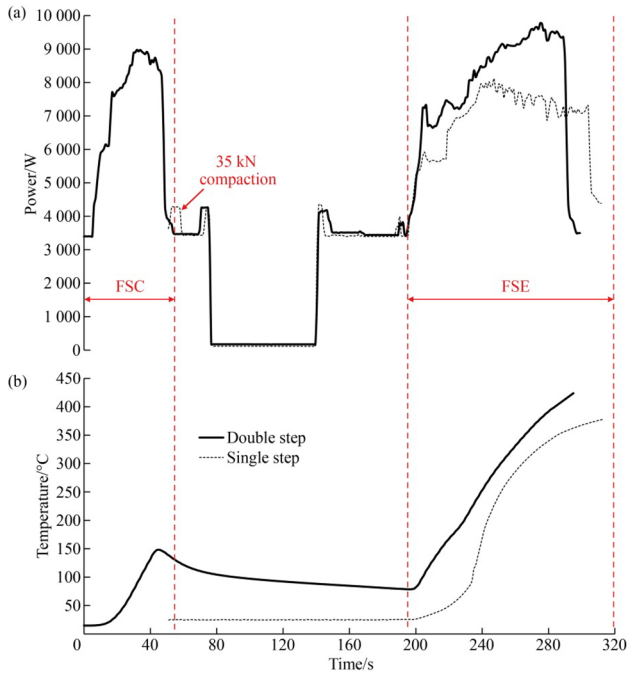


**Fig. 20** **a** Power consumption and **b** temperature comparison between double and single step

of primary aluminum), and extrusion was about 40 MJ/kg. These results clearly demonstrate that FSE, at the optimal parameters (C5), provides significant energy saving.

In order to provide insight into the single step extrusion efficiency in terms of less power demanding, a comparison between two scenarios was carried out. Specifically, a case study where the tube was directly extruded from chips and a case study where the chips were first consolidated into a billet and then extruded were studied. For consolidating the chips into a billet, a friction stir consolidation process was selected. This process is a suitable option because it shares the same setup and mechanism and the process dynamics of FSE, but no extrusion is provided during FSC. In fact, the FSC involves the use of a die, a backing plate and a tool which, in this study, were the same of the compacting phase.

The process parameters selected for the billet consolidation were chosen on the basis of previous research [29, 30]; specifically, 1 500 r/min (rotational speed) and 15 kN (vertical load) were selected. Results of the comparison between the two scenarios applied to the C5 case study are depicted in Fig. 20. It is clear that the single step is more energy efficient as the consolidation step is skipped. Moreover, in the single step process the material is less consolidated at the beginning, resulting in a lower power required for extruding the tube. In fact, looking only at the extrusion step, it is possible to notice that the double step demands a lower power level with respect to the single step approach. In conclusion, the here proposed single step approach is an environmentally friendly solution with respect to the double step as it requires both reduced power level and shorter processing time.

Concerning the temperature profiles, the extrusion step performed after the FSC process resulted in an excessive temperature increase. The recorded temperature trends of the entire working cycle of the two approaches are reported, as shown in Fig. 20.

## 4 Conclusions

The aim of this work was to produce aluminum tubes directly from chips using single step FSE process. An experimental campaign was performed to successfully produce consolidated tube from AA2024-O aluminum chips under various process conditions, and a numerical approach was employed to better explore the process mechanics. The mechanical and metallurgical properties of the tubes were analyzed, and the following conclusions could be drawn.

(i) This study successfully demonstrated the single-step production of aluminum tubes, directly from chips, achieving excellent mechanical and microstructural properties while ensuring superior energy efficiency compared to conventional multi-step routes.

(ii) The microstructural analysis shows that strong grain refinement is obtained with small grain size variation in radial direction (average grain size equal to 4): 3.4 μm close to the inner surface, 4.4 μm at the middle of the thickness and 3.5 μm close to the outer surface.

(iii) Defects such as porosity and cracks have been observed on low heat input conditions (1 000 r/min-12 kN). On the contrary, hot cracks phenomena were observed at high heat input (2 000 r/min-15 kN). A quantitative study demonstrated that the porosity of the extruded tube at worst condition (1 000 r/min) resulted in 1.8% of porosity.

(iv) Microhardness increased significantly compared to the base material (from 61.5 HV to an average 140 HV). Moreover, it has been observed that the hardness increases with increasing the vertical load.

(v) Compression and flattening tests confirmed that the 1 500 r/min-15 kN condition yielded the best bonding and mechanical performance, compared to 1 000 and 2 000 r/min, showing no separation of the layers during the flattening of the tubes, and good bonding efficacy of the process.

(vi) The numerical simulation corroborated the finding concerning grain size. Zener-Hollomon parameter

was calculated and high Zener-Hollomon values were observed at the internal and external surface of the tube, which was in accordance with the experimental grain size measurements. Moreover, the tool's stirring effect on the recrystallization phenomenon was successfully explained and justified by strain study thanks to numerical simulations.

(vii) Energy analysis confirmed that the single-step approach was more efficient and environmentally friendly than the traditional two-step route, as it required both reduced power level and shorter processing time. Additionally, the FSE revealed an SEC of about 15 MJ/kg at C5 conditions, which was lower than the traditional melting + extrusion process.

(viii) Experimental and numerical results revealed that excessive consolidation of the material in the bottom region of the extrusion chamber might represent a process limit. A solid bonding analysis demonstrated that the unprocessed material was affected by pressure and temperature, leading to earlier consolidation. As a matter of fact, the required extrusion force increases as the material consolidates, leading to an excessive temperature increase and a reduction of the extrusion rate.

Future work will be performed to improve the FSE setup aiming to solve the issue of the excessive temperature increase by operating the solutions discussed in this paper. Also, the possibility of producing multi-material tubes from different aluminum alloy chips will be tested. Lastly, a continuous FSE process, already explored by authors for wire production, will be implemented in tube manufacturing in order to propose industrial scale applications.

**Acknowledgment** This study was funded by Italian MUR funds through European Union-NEXT Generation EU scheme (Grant No. B53D23006550006).

**Funding** Open access funding provided by Università degli Studi di Palermo within the CRUI-CARE Agreement.



## References

1. Brown KR, Venie MS, Woods RA (1995) The increasing use of aluminum in automotive applications. JOM 47:20–23. https://doi.org/10.1007/BF03221224
2. Zhang Y, Sun M, Hong J et al (2016) Environmental footprint of aluminum production in China. J Clean Prod 133:1242–1251. https://doi.org/10.1016/j.jclepro.2016.04.137
3. Krishnan PK, Christy JV, Arunachalam R et al (2019) Production of aluminum alloy-based metal matrix composites using scrap aluminum alloy and waste materials: influence on microstructure and mechanical properties. J Alloys Compd 784:1047–1061. https://doi.org/10.1016/j.jallcom.2019.01.115
4. Al-Alimi S, Shamsudin S, Yusuf NK et al (2022) Recycling aluminium AA6061 chips with reinforced boron carbide (B4C) and zirconia ($ZrO_2$) particles via hot extrusion. Metals 12(8):1329. https://doi.org/10.3390/met12081329
5. Tekkaya AE, Schikorra M, Becker D et al (2009) Hot profile extrusion of AA-6060 aluminum chips. J Mater Process Technol 209(7):3343–3350. https://doi.org/10.1016/j.jmatprotec.2008.07.047
6. Wan B, Chen W, Lu T et al (2017) Review of solid state recycling of aluminum chips. Resour Conserv Recycl 125:37–47
7. Chen Y, Liu H, Wu Y et al (2024) Comparative study of the microstructure evolution and mechanical properties of Zn-0 1Mg-0 02Ca alloy under cold rolling and ECAP. Mater Sci Eng A 908:146765. https://doi.org/10.1016/j.msea.2024.146765
8. Whalen S, Overman N, Joshi V et al (2019) Magnesium alloy ZK60 tubing made by shear assisted processing and extrusion (ShAPE). Mater Sci Eng A 755:278–288. https://doi.org/10.1016/j.msea.2019.04.013
9. Suzuki K, Huang XS, Watazu A et al (2007) Recycling of 6061 aluminum alloy cutting chips using hot extrusion and hot rolling. Mater Sci Forum 544/545:443–446. https://doi.org/10.4028/www.scientific.net/msf.544-545.443
10. Buffa G, Baffari D, Ingarao G et al (2020) Uncovering technological and environmental potentials of aluminum alloy scraps recycling through friction stir consolidation. Int J Precis Eng Manuf Green Technol 7(5):955–964
11. Paraskevas D, Vanmeensel K, Vleugels J et al (2014) Spark plasma sintering as a solid-state recycling technique: the case of aluminum alloy scrap consolidation. Materials 7(8):5664–5687. https://doi.org/10.3390/ma7085664
12. Zhang S, Frederick A, Wang Y et al (2019) Microstructure evolution and mechanical property characterization of 6063 aluminum alloy tubes processed with friction stir back extrusion. JOM 71(12):4436–4444. https://doi.org/10.1007/s11837-019-03852-7
13. Buffa G, Campanella D, Adnan M et al (2024) Improving the industrial efficiency of recycling aluminum alloy chips using friction stir extrusion: thin wires production process. Int J Precis Eng Manuf Green Technol 11(4):1133–1146. https://doi.org/10.1007/s40684-023-00573-w
14. Baffari D, Reynolds AP, Masnata A et al (2019) Friction stir extrusion to recycle aluminum alloys scraps: energy efficiency characterization. J Manuf Process 43:63–69. https://doi.org/10.1016/j.jmapro.2019.03.049
15. Adnan M, Buffa G, Baghdadchi A et al (2024) Unveiling the mechanical and microstructural properties of SiC reinforced aluminum wires recycled from scraps by friction stir extrusion. Mater Sci Eng A 916:147333. https://doi.org/10.1016/j.msea.2024.147333

16. Sharifzadeh M, Ali Ansari M, Narvan M et al (2015) Evaluation of wear and corrosion resistance of pure Mg wire produced by friction stir extrusion. Trans Nonferrous Met Soc China 25(6):1847–1855
17. Milner JL, Abu-Farha F (2014) Microstructural evolution and its relationship to the mechanical properties of Mg AZ31B friction stir back extruded tubes. In: magnesium technology 2014, Springer International Publishing, Cham, pp 263–268
18. Zhang Z, Liang J, Xia T et al (2023) Effects of oxide fragments on microstructure and mechanical properties of AA6061 aluminum alloy tube fabricated by thermomechanical consolidation of machining chips. Materials 16(4):1384. https://doi.org/10.3390/ma16041384
19. Behnagh RA, Fathi F, Yeganeh M et al (2019) Production of seamless tube from aluminum machining chips via double-step friction stir consolidation. Int J Adv Manuf Technol 104(9):4769–4777. https://doi.org/10.1007/s00170-019-04326-5
20. Mohebbi MS, Akbarzadeh A (2010) Accumulative spin-bonding (ASB) as a novel SPD process for fabrication of nanostructured tubes. Mater Sci Eng A 528(1):180–188. https://doi.org/10.1016/j.msea.2010.08.081
21. Farshidi MH, Kazeminezhad M, Miyamoto H (2014) Microstructrual evolution of aluminum 6061 alloy through tube channel pressing. Mater Sci Eng A 615:139–147. https://doi.org/10.1016/j.msea.2014.07.061
22. Arzaghi M, Fundenberger JJ, Toth LS et al (2012) Microstructure, texture and mechanical properties of aluminum processed by high-pressure tube twisting. Acta Mater 60(11):4393–4408. https://doi.org/10.1016/j.actamat.2012.04.035
23. Mesbah M, Faraji G, Bushroa AR (2014) Characterization of nanostructured pure aluminum tubes produced by tubular channel angular pressing (TCAP). Mater Sci Eng A 590:289–294. https://doi.org/10.1016/j.msea.2013.10.036
24. Whalen S, Taysom BS, Overman N et al (2023) Porthole die extrusion of aluminum 6063 industrial scrap by shear assisted processing and extrusion. Manuf Lett 36:52–56. https://doi.org/10.1016/j.mfglet.2023.01.005
25. Abu-Farha F (2012) A preliminary study on the feasibility of friction stir back extrusion. Scr Mater 66(9):615–618. https://doi.org/10.1016/j.scriptamat.2012.01.059
26. Swarnkar R, Karmakar S, Pal SK (2023) An investigation of bimetallic tube fabrication through a novel friction stir extrusion based technology for automotive applications. Mater Today Commun 35:106363. https://doi.org/10.1016/j.mtcomm.2023.106363
27. Asadi P, Akbari M, Sadowski T et al (2024) Examining the impact of tool taper angle in Al-Si tube manufacturing by friction stir extrusion. J Manuf Process 131:532–544. https://doi.org/10.1016/j.jmapro.2024.09.047
28. Strodick S, Schmidt R, Gerdes L et al (2021) Impact of cutting parameters on the mechanical properties of BTA deep drilled components under quasi-static compression. Procedia CIRP 103:207–212. https://doi.org/10.1016/j.procir.2021.10.033
29. Puleo R, Latif A, Ingarao G et al (2024) A generalized parametric model for the bonding occurrence prediction in friction stir consolidation of aluminum alloys chips. J Manuf Process 131:604–618. https://doi.org/10.1016/j.jmapro.2024.09.049
30. Puleo R, Latif A, Ingarao G et al (2023) Solid bonding criteria design for aluminum chips recycling through friction stir consolidation. J Mater Process Technol 319:118080. https://doi.org/10.1016/j.jmatprotec.2023.118080
31. Baffari D, Reynolds AP, Li X et al (2017) Influence of processing parameters and initial temper on friction stir extrusion of 2050 aluminum alloy. J Manuf Process 28:319–325. https://doi.org/10.1016/j.jmapro.2017.06.013
32. Baffari D, Buffa G, Campanella D et al (2017) Process mechanics in friction stir extrusion of magnesium alloys chips through experiments and numerical simulation. J Manuf Process 29:41–49. https://doi.org/10.1016/j.jmapro.2017.07.010
33. Latif A, Gucciardi M, Ingarao G et al (2022) Outlining the limits of friction stir consolidation as used as an aluminum alloys recycling approach. In: smart innovation, systems and technologies. Springer Science and Business Media Deutschland GmbH, pp 169–180
34. Chang CI, Lee CJ, Huang JC (2004) Relationship between grain size and Zener-Holloman parameter during friction stir processing in AZ31 Mg alloys. Scr Mater 51(6):509–514. https://doi.org/10.1016/j.scriptamat.2004.05.043
35. Huda Z, Zaharinie T (2009) Kinetics of grain growth in 2024–T3: an aerospace aluminum alloy. J Alloys Compd 478(1/2):128–132. https://doi.org/10.1016/j.jallcom.2008.11.071
36. Donati L, Tomesani L (2004) The prediction of seam welds quality in aluminum extrusion. J Mater Process Technol 153:366–373. https://doi.org/10.1016/j.jmatprotec.2004.04.215
37. Cooper DR, Song J, Gerard R (2018) Metal recovery during melting of extruded machining chips. J Clean Prod 200:282–292. https://doi.org/10.1016/j.jclepro.2018.07.246



**Muhammad Adnan** is a doctor in Mechanical, Manufacturing, Management and Aerospace Innovation at University of Palermo. He received his master's degree in Mechanical Engineering from Dalian University of Technology (DUT), China in 2021 and bachelor degree from University of Engineering and Technology (UET), Lahore Pakistan in 2018. His research focuses on methods, solutions, and numerical models for the solid-state recycling process and solid-state joining process.

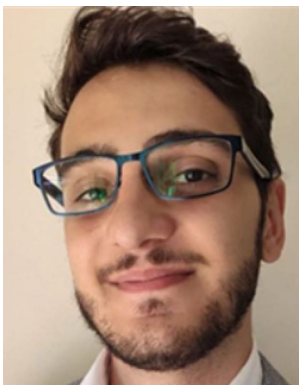

**Riccardo Puleo** received his a Ph.D. in Mechanical, Manufacturing, Management and Aerospace Innovation, from University of Palermo (UniPa), in 2025. He received his bachelor's and master's degrees in Mechanical Engineering from University of Palermo on solid state welding techniques. His main field is the study of the solid bonding phenomena in metal scrap recycling, with a focus on numerical simulation of friction stir-based recycling processes.

**Gianluca Buffa** received his Ph.D. in Industrial and Production Engineering from University of Palermo in 2007. Currently he is a full professor of Manufacturing at University of Palermo. He is coauthor of more than 180 papers, published in peer reviewed international journals and conference proceedings, book chapters and a patent.

**Livan Fratini** graduated with honours in Mechanical Engineering in 1993 and took his Ph.D. in Production Engineering in 1997. Currently he is pa rofessor at University of Palermo. He was awarded a young researcher travel award by the Japan Society for Technology of Plasticity (2000) and the F.W. Taylor Medal by the CIRP (2007). Fratini has been involved in several research projects on metal forming topics, and is coauthor of about 330 papers on international scientific journals.

**Giuseppe Ingarao** received a M.Sc. degree in Management Engineering and a Ph.D. in Industrial Engineering and Management from University of Palermo. He is currently a full professor at University of Palermo. His research focuses on sustainable manufacturing. Specifically, he deals with the design of energy- and resource-efficient metal shaping processes (additive, subtractive and mass conserving), methods and techniques for life cycle assessment of metal components, and innovative metal recycling processes.